Three-dimensional Structure of Nanocrystals from High-energy X-ray Diffraction and Atomic Pair Distribution Function Analysis

V. Petkov

Department of Physics, Central Michigan University, Mt. Pleasant, MI 48858, USA,
petkov@phy.cmich.edu

ABSTRACT

The atomic Pair Distribution Function (PDF) analysis and high-energy x-ray diffraction are introduced as a tool for determining the three-dimensional structure of nanocrystalline materials. The great potential of this experimental approach is demonstrated with results from successful studies on $(Polyaniline)_xV_2O_5nH_2O$ nanocomposites and dendrimer stabilized gold nanoparticles. We find that $(Polyaniline)_xV_2O_5nH_2O$ has a lamellar-type structure wherein polymeric chains are sandwiched between double layers of $V\text{-}O_6$ octahedra. Gold nanoparticles possess a distorted face centered cubic-type structure with the degree of distortion increasing with the decrease in particle's size.

Keywords: x-ray diffraction, nanocomposites, nanoparticles, structure

1 INTRODUCTION

Knowledge of the atomic-scale structure is an important prerequisite to understand and predict the properties of materials. In the case of crystals it is obtained from the positions and intensities of the Bragg peaks in the diffraction patterns. However, materials constructed at the nanoscale lack the translational symmetry and long-range order of perfect crystals. The diffraction patterns of such materials show only a few Bragg peaks, if any, and a pronounced diffuse component. This poses a real challenge to the usual techniques for structure determination. The challenge can be met by employing the so-called atomic Pair Distribution Function (PDF) analysis and high energy x-ray diffraction. This non-traditional experimental approach takes into account both Bragg and diffuse scattering and yields the atomic structure in terms of a small set of parameters such as a unit cell and atomic coordinates [1-4].

The reduced atomic Pair Distribution Function, $G(r)$, is defined as follows:

$$G(r) = 4\pi r[\rho(r) - \rho_0] \qquad (1)$$

where $\rho(r)$ and ρ_0 are the local and average atomic number densities, respectively, and r is the radial distance. It peaks at characteristic distances separating pairs of atoms and thus reflects the atomic-scale structure. The PDF $G(r)$ is the Fourier transform of the experimentally observable total structure function, $S(Q)$, i.e.,

$$G(r) = (2/\pi)\int_{Q=o}^{Q_{max}} Q[S(Q) - 1]\sin(Qr)dQ \qquad (2)$$

where Q is the magnitude of the wave vector ($Q = 4\pi \sin\theta/\lambda$), 2θ is the angle between the incoming and scattered radiation beams and λ is the wavelength of the radiation used. The structure function is related to the coherent part of the total intensity diffracted from the material as follows:

$$S(Q) = 1 + \left[I^{coh}(Q) - \sum c_i |f_i(Q)|^2\right] / \left|\sum c_i f_i(Q)\right|^2 \qquad (3)$$

where $I^{coh}(Q)$ is the coherent scattering intensity per atom in electron units and c_i and f_i are the atomic concentration and x-ray scattering form factor, respectively, for the atomic species of type i [5]. As can be seen from Eqs. 1-3, the PDF is simply another representation of the powder diffraction data. However, exploring the diffraction data in real space is advantageous, especially in the case of materials of limited structural coherence. First, as Eq. 2 implies the *total* scattering, including Bragg scattering as well as diffuse scattering, contributes to the PDF. Therefore both the longer-range atomic structure, responsible for the sharp Bragg-like diffraction features, and the local non-periodic structural imperfections, resulting in the diffuse component of the diffraction pattern, are contained in the PDF. Second, by accessing high values of Q, experimental PDFs with improved real-space resolution can be obtained and hence, quite fine structural features can be revealed. In fact, data at high Q values (Q>10 Å^{-1}) are critical to the success of PDF analysis. Third, the PDF is less affected by diffraction optics and experimental factors since these are accounted for when extracting the coherent intensities from the raw diffraction data. This renders the PDF a structure-dependent quantity that gives directly relative positions of atoms in materials and enables convenient testing and refinement of structural models. The great potential of the PDF technique is well demonstrated by the results presented below.

2 EXAMPLES OF PDF STUDIES

2.1 Atomic ordering in (Polyaniline)$_x$V$_2$O$_5$nH$_2$O

In recent years, conducting polymeric nanocomposites have attracted much attention because of their unique and novel properties and a wide variety of potential applications. Of particular interest are nanocomposites based on polyaniline (PANI) which find applications in solar cells, biosensors and color displays [6]. A prime example of the family of PANI-based nanocomposites is (PANI)$_x$V$_2$O$_5$nH$_2$O. Here the combination of the conducting properties of PANI and the inorganic host, V$_2$O$_5$nH$_2$O xerogel, results in a nanomaterial with interesting charge- and ion-transport characteristics [7]. No simulations and theoretical studies on the physical properties of the material are done so far mainly because its nanocrystalline state made it difficult to determine the atomic-scale structure in detail.

The (PANI)$_x$V$_2$O$_5$nH$_2$O system is composed of two components neither of which exists in a crystalline form. The V$_2$O$_5$nH$_2$O xerogel is nanocrystalline in nature and its structure was unknown ever since the material was discovered in the beginning of the last century. Recently, we determined its atomic-scale structure [4] using the only technique currently available that can do so, namely the PDF technique. Polyaniline is a poorly crystalline material whose three-dimensional structure has never been determined in detail. Here we build upon our previous results and the capabilities of the PDF technique to elucidate the structure of (PANI)$_x$V$_2$O$_5$nH$_2$O. The synthesis of the nanocomposite is described in full detail in ref. [4]. X-ray diffraction (XRD) experiments were carried out at the beamline X7a at the National Synchrotron Light Source at Brookhaven National Laboratory using x-rays of energy 29.09 keV (λ = 0.4257). The higher energy x-rays were used to obtain diffraction data to higher values of the wave vector, *Q*, which is important for the success of PDF analysis. The experimental diffraction patterns for nanocrystalline (PANI)$_x$V$_2$O$_5$nH$_2$O, crystalline V$_2$O$_5$ and pure polyaniline are shown in Fig.1. The latter two materials were used as standards. As can be seen, the XRD pattern of crystalline V$_2$O$_5$ exhibits well-defined Bragg peaks up to Q ~ 10 Å^{-1}. The material is obviously a well-ordered crystalline solid. In contrast, the Bragg peaks in the XRD patterns of nanocrystalline (PANI)$_{0.5}$V$_2$O$_5$nH$_2$O are rather broad and merge into a slowly oscillating diffuse component already at Q values as low as 4-5 Å^{-1}. The diffraction pattern of polyaniline is even less structured: it shows only one sharp feature at low Q values - a behavior typical for severely disordered materials. Such diffraction patterns are very difficult to analyze using ordinary techniques for structure determination. However, when reduced to the corresponding atomic PDFs, they become a structure-sensitive quantity lending itself to structure determination and modeling. The experimental PDF for nanocrystalline (PANI)$_{0.5}$V$_2$O$_5$nH$_2$O is shown in Fig. 2.

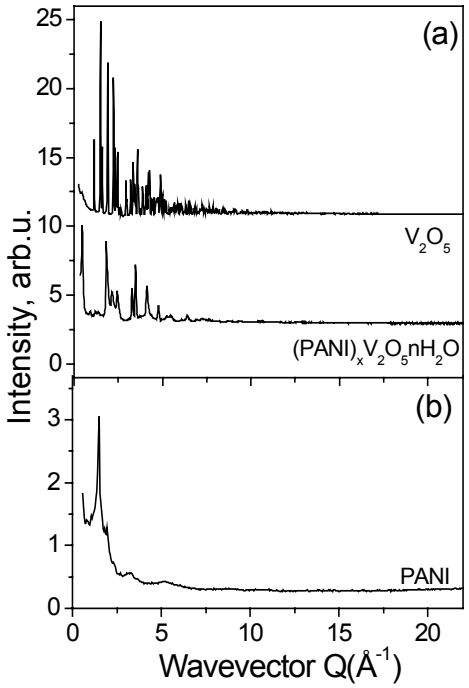

Figure 1. Diffraction patterns of (a) nanocrystalline (PANI)$_x$V$_2$O$_5$nH$_2$O and crystalline V$_2$O$_5$ and (b) polyaniline.

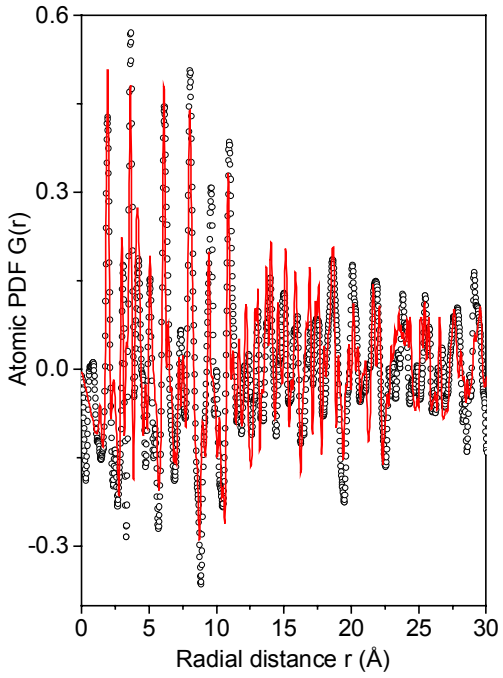

Figure 2. Comparison between the experimental (open circles) and model (solid line, in red) PDFs for (PANI)$_x$V$_2$O$_5$nH$_2$O. The experimental PDF is extracted from the diffraction data shown in Fig. 1. The model PDF is calculated from the atomic configuration shown in Fig. 3.

It shows a series of well-defined peaks each corresponding to a particular set of frequently occurring interatomic

distances. Several structural models were tested against the experimental PDF data [8]. The parameters of the models, including unit cells and positions of the atoms in them, were refined as to obtain as good as possible agreement between the experimental and model PDF data. The best model found reproduces the experimental PDF data very well as can be seen in see Fig. 2. The model features the nanocomposite as an assembly of V_2O_5 bilayers enclosing densely packed PANI chains. A fragment of the model is presented in Fig. 3. The parameters of the model, including coordinates of the individual atoms (476 in total) are listed in ref. [8]. The model is periodic and of relatively small size, given the complexity of the nanomaterial studied, thereby allowing the exploration of structure-property relationships in $(PANI)_xV_2O_5nH_2O$. It describes the nanocomposite as an intimate mix of V_2O_5 bilayers and PANI chains, whose nominal planes are perpendicular to the layers, and corroborates the conclusions drawn in previous studies [7]. It is likely that the model misses some subtle details of the atomic structure in the nanocomposite as, for example, the likely presence of NH-O-V hydrogen bonding between the PANI chains and the V_2O_5 matrix and a possible "freezing" of some of the PANI chains inside the constrained interlayer space. Therefore, the model should be considered and used with care bearing in mind that it is still an approximation to the structure of $(PANI)_xV_2O_5nH_2O$. More subtle details as the ones mentioned above may be tested and explored by using structural information provided by local probes and spectroscopic techniques such as EPR, NMR, IR, Raman etc. This structural level of detail goes beyond the scope of the present study. The recent progress in experimental and computational techniques, however, make such an experimental approach feasible, in particular in cases where the more detailed local structural information is known to be critical for improving the properties of a nanocomposite material.

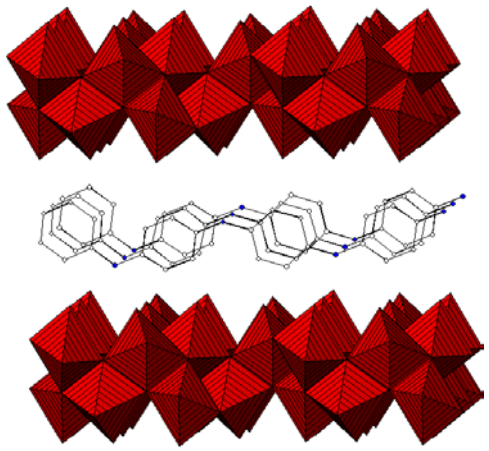

Figure 3. Atomic ordering in $(PANI)_xV_2O_5nH_2O$ as determined by the present PDF studies. The vanadium-oxygen octahedra (in red) are assembled in bilayers and the polyaniline chains occupy the interlayer space.

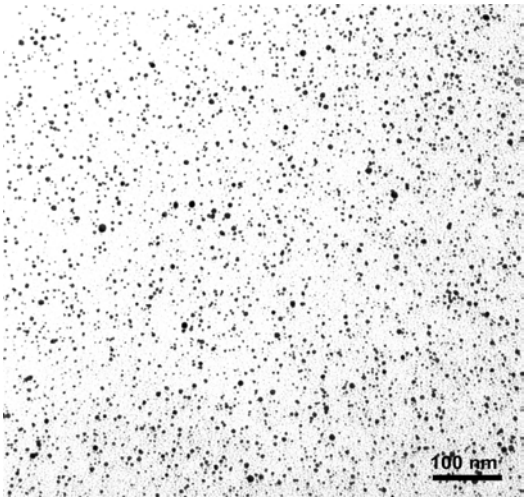

Figure 4. TEM image of dendrimer stabilized 2 nm gold nanoparticles.

2.2 Atomic ordering in dendrimer stabilized gold nanoparticles

The plasmonics of gold nanoparticles is the subject of intense research and has found many uses, ranging from sensors to optical materials [9]. In general, the surface plasmon resonance of gold nanoparticles is controlled by many factors, including their structure and size. We undertook a structure study on dendrimer stabilized gold nanoparticles of sizes 2nm, 12 nm and 30 nm to reveal this interrelation. The particles were made following a procedure described in [10]. An electron microscopy image of the nanoparticles of size 2 nm is shown in Fig. 4. The particles are spherical in shape and well separated from each other thanks to the capping layer of poly(amidoamine) dendrons. X-ray diffraction (XRD) experiments were carried out at the beamline 11IDC at the Advanced Photon Source at the Argonne National Laboratory using X-rays of energy 115.23 keV (λ = 0.1076 Å). The nanoparticles were suspended in water and sealed in glass capillaries. In addition, pure gold (in powder) was measured and used as a standard. The experimental atomic PDFs are shown in Fig. 5. The PDF for bulk gold shows well defined peaks to very long real space distances reflecting the presence of a 3D periodicity and long-range order in this crystalline material. The experimental data are well fit by a model based on the face centered cubic (fcc) structure of crystalline gold as can be seen in Fig. 5. The experimental PDFs for the gold nanoparticles decay to zero at much shorter real space distances reflecting the reduced degree of structural coherence in these nanomaterials. As can be expected this degree diminishes with the particle's size. A comparison between the experimental data and model ones based on the fcc-type structure shows that the atomic ordering in the

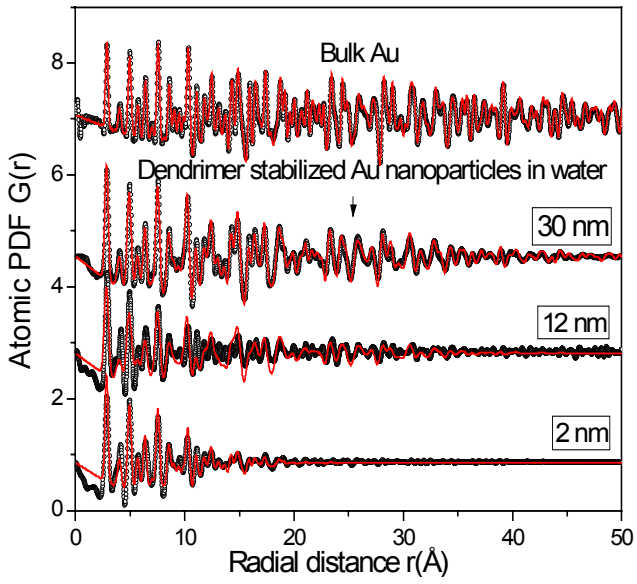

Figure 5. Experimental (circles) atomic PDFs for bulk crystalline gold and dendrimer stabilized gold nanoparticles of different sizes. Model PDFs based on a fcc type structure are shown as solid lines (in red).

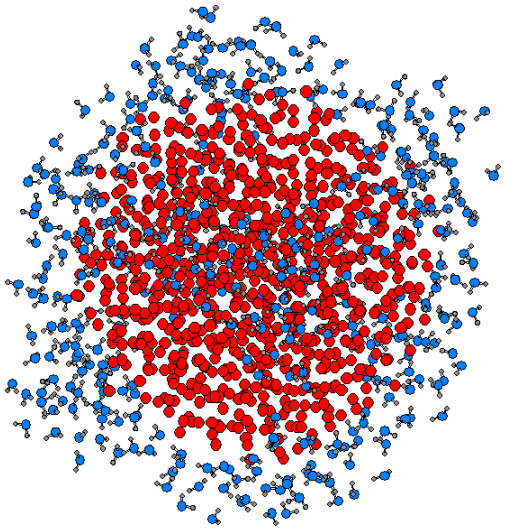

Figure 6. Model of a 2 nm gold nanoparticle (gold atoms are shown as circles in red) surrounded by water (in blue) molecules.

nanoparticles bears resemblance to that occurring crystalline gold (see Fig. 5). To determine the 3D structure of the nanoparticles in detail we generated model atomic configurations by Monte Carlo simulations employing realistic interatomic potentials. A model representing a 2 nm gold nanoparticle in water is shown in Fig. 6. The model reproduces the experimental PDF data quite well and allows the exploration of the structure-sensitive properties of this useful nanomaterial. Modeling studies of 12 nm and 30 nm gold nanoparticles are under way.

3. CONCLUSION

The three-dimensional structures of the scientifically and technologically important $(Polyaniline)_xV_2O_5nH_2O$ nanocomposites and dendrimer stabilized gold nanoparticles have been determined by the PDF technique. The structures are given in terms of a small number of sensible parameters, including atomic coordinates. This development opens up the route to better explaining, predicting, and possibly improving the properties of these materials by using both theoretical and experimental tools. Also, the results of the present study are a direct demonstration of the ability of the PDF technique to yield three-dimensional structural information for materials of limited structural coherence, including nanostructured materials. The technique succeeds because it relies on total scattering data obtained from the material, and as a result, is sensitive to its essential structural features. This allows a convenient testing and refining of structural models. Furthermore, the technique probes the bulk and can provide an important foundation to imaging techniques such as transmission electron and atomic force microscopy, which reveal only structural features projected down one axis or a surface.

ACKNOWLEDGMENTS Thanks are due to Tom Vogt, Yang, Ren, Mercouri Kanatzidis, Donald Tomalia and Baohua Huang for help with the sample preparation and/or the synchrotron radiation experiments. The work was supported by NSF through grant DMR 304391(NIRT) and ARL through grant DAAD19-03-2-0012.

REFERENCES

1. V. Petkov, P. Y. Zavalij, S. Lutta, M. S. Whittingham, V. Parvanov and S. Shastri, *Phys. Rev. B* ***69***. (2004) 085410.
2. V. Petkov, S.J.L. Billinge, T .Vogt, A.S. Ichimura and J.L. Dye, *Phys. Rev. Lett.* **89** (2002) 075502.
3. M. Gateshki, S-J Hwang, D. Hoon Park, Y. Ren, and V. Petkov, *Chem. Mater.,* **16** (2004) 5153.
4. V. Petkov, E. Bozin, S.J.L. Billinge, P. Trikalitis, M. Kanatzidis and T. Vogt,, *J. Am. Chem. Soc*. **124** (2002) 10157.
5. P.H. Klug, and L.A. Alexander, *X-ray Diffraction Procedures for Polycrystalline Materials* (Wiley, New York, 1974).
6. J.M. Zeh, S.J. Liou, C.Y. Lai, C. Wu, C*hem. Mater*., **13** (2001) 1131; J. Wu , Y.H. Zou; H.L. Li, G.L. Shen, R.Q. Yu, *Sensors and Actuators B* **104** (2005) 43.
7. .M.G. Kanatzidis, C.G. Wu, M. Ho, C.R. Kannefurf, *J. Am. Chem. Soc*., **111** (1989) 4139.
[8] V. Petkov, V. Parvanov, P. Trikalitis, Ch. Malliakas, T.Vogt and M. Kanatzidis, *J. Am. Chem. Soc*. (2005), submitted.
[9] S. Srivastava, B. L. Frankamp and V.M. Rotello, *Chem. Mater*. **17** (2005) 487.
[10] V. Petkov, Y. Peng, B. Huang and D. Tomalia, in preparation.